Published in final edited form as:
J Cataract Refract Surg. 2014 June ; 40(6): 1021–1031. doi:10.1016/j.jcrs.2013.09.022.

Spatially heterogeneous corneal mechanical responses before and after riboflavin–ultraviolet-A crosslinking

Joel R. Palko, MD, **Junhua Tang, PhD**, **Benjamin Cruz Perez, MS**, **Xueliang Pan, PhD**, and **Jun Liu, PhD**

College of Medicine (Palko), the Department of Biomedical Engineering (Tang, Perez, Liu), the Center for Biostatistics (Pan), and the Department of Ophthalmology (Liu), Ohio State University, Columbus, Ohio, USA

Abstract

PURPOSE—To determine the heterogeneous through-thickness strains in the cornea at physiologic intraocular pressures before and after corneal collagen crosslinking (CXL) using noninvasive ultrasound.

SETTING—Department of Biomedical Engineering, Ohio State University, Columbus, Ohio, USA.

DESIGN—Experimental study.

METHODS—Sixteen paired canine corneoscleral shells were divided into 2 groups. The CXL group completed a standard CXL protocol using riboflavin–ultraviolet-A (UVA) irradiation. The control group was given an identical treatment except UVA irradiation. Ultrasound scans (at 55 MHz) of the cornea were obtained before and after treatment as the corneoscleral shell was inflated from 5 mm Hg to 45 mm Hg to calculate the distributive through-thickness strains in the cornea. The mean radial and tangential strains of the whole cornea layer, as well as those of the anterior, middle, and posterior thirds of the cornea, were compared before and after treatment in the control group and CXL group using linear mixed models with repeated measures.

RESULTS—Significant reductions in tangential and radial strains occurred in the CXL group (P=.003 and P=.0025, respectively) but not the control group (P=.08 and P=.63, respectively). The anterior third had the smallest strains in all pretreated corneas (P<.001) and posttreated corneas (CXL group, P=.023; control group, P=.01).

CONCLUSIONS—Ultrasound speckle tracking showed heterogeneous strain distributions through the cornea and confirmed that CXL results in a stiffer corneal response (ie, smaller strains during physiologic loadings). This technique may provide a clinical tool to quantify the biomechanical effects of CXL.

Financial Disclosure—No author has a financial or proprietary interest in any material or method mentioned.

Corresponding author: Jun Liu, PhD, 270 Bevis Hall, 1080 Carmack Road, Columbus, Ohio, USA. liu.314@osu.edu.

Presented as a poster at the annual meeting of the Association for Research in Vision and Ophthalmology, Seattle, Washington, USA, May 2013.

Crosslinking of the cornea's extracellular matrix (ECM) has provided a new therapy for keratoconus, presumably by manipulating the cornea's biomechanical properties and altering its susceptibility to degradation by matrix metalloproteinases.[1–4] Corneal collagen crosslinking (CXL) has the potential to be a treatment option not only for keratoconus but also for ocular conditions such as corneal ectasia after laser in situ keratomileusis, alkali burns of the cornea, and infectious keratitis.[5–8] However, a better understanding of the biomechanical effects of CXL is required to optimize this treatment. It has been suggested that the CXL within the cornea using the clinical standard riboflavin and ultraviolet-A (UVA) technique occurs via mechanisms that involve the photochemically generated riboflavin triplets and singlet oxygen.[9,10] These reactive agents are thought to induce variable types of crosslinking in the ECM encompassing collagen and proteoglycan core proteins.[11] The increased chemical bonding between corneal microstructural components is believed to strengthen the tissue mechanically and reduce its susceptibility to enzymatic degradations.[4,12–15]

The ability to repeatedly, accurately, and nondestructively monitor an in vivo biomechanical metric of the cornea that is affected by CXL would allow for better clinical assessment of the treatment and provide a tool to catalyze the further development of the therapy. Clinical studies have quantified the effects of CXL using measures such as refraction, visual acuity, and corneal topography.[1,16] However, these clinical parameters may not be ideal for monitoring the immediate and progressive biophysical changes associated with CXL. By measuring the mechanical changes caused by CXL, a more fundamental level of data can be obtained to objectively characterize the effects of the therapy. Such a metric may provide a better understanding of the CXL mechanism, allow for improved evaluations of new CXL methods, and potentially offer an approach to more individualized patient care.[17]

Characterizing the mechanics of the cornea after CXL with the Ocular Response Analyzer (Reichert Technologies) using parameters such as corneal hysteresis and the corneal resistance factor did not yield consistent findings.[18,19] In the past, our laboratory has used noninvasive ultrasonic spectroscopy to quantify the mechanical changes in the crosslinked corneas using the parameter of aggregate modulus.[14] These approaches do not provide enough spatially resolved detail of the heterogeneous mechanical properties of the cornea before and after CXL treatment.[5] Recent studies have attempted to address this challenge and develop noninvasive techniques to image the spatial distribution of corneal biomechanical properties. For example, optical coherence tomography has been used to generate 2-dimensional (2-D) maps of heterogeneous corneal displacements in response to the compression from a gonioscopy lens.[20] Brillouin microscopy has been used to measure the 3-dimensional (3-D) interaction of light with intrinsic thermodynamic fluctuations (known as acoustic phonons) in bovine corneas.[21] This photon–phonon interaction is characterized by a frequency shift in Brillouin-scattered light that is related to the longitudinal elastic modulus of the tissue. Preliminary studies[22] using this method in ex vivo bovine corneas have shown the feasibility of detecting the effects of different CXL protocols. High-frame-rate ultrasound (US) at 15 MHz has been used to image shear wave propagations induced by ultrasonic radiation force and has shown the feasibility of obtaining 2-D and 3-D elastic maps of the corneal surface as a potential way to noninvasively analyze

the mechanical changes occurring in the cornea after CXL.[23] The US elasticity microscope has also been used to map strains in porcine corneas that were subject to slit deformations.[24]

In this study, we used a high-frequency US speckle tracking technique[25] to quantify the intraocular pressure (IOP)–induced distributive strains of different cross-sections of the cornea before and after CXL. This technique measures the displacements of ultrasonic speckles within the cornea during IOP elevations, providing direct delineation of the local deformations in response to physiologic loadings to characterize the heterogeneous mechanical responses of the cornea. Paired canine eyes were used in this study to examine the strains before and after CXL or a sham treatment without UVA irradiation.

MATERIALS AND METHODS

Canine Globe Preparation

Sixteen globes from 8 dogs of mixed breeds and ages were collected from a local animal shelter. The posterior third of the globe was dissected, and the interior contents of the eyes were removed within 60 minutes after the dogs were humanely killed. The remaining anterior corneoscleral shell was immediately placed in a corneal storage medium (Optisol GS, Bausch & Lomb) to prevent cornea swelling and maintain tissue integrity. The posterior border of the corneoscleral shell was then clamped and sealed to a purpose-designed pressure chamber. The chamber was connected to a pressure control system consisting of a syringe pump (UltraPhD, Harvard Apparatus) and a pressure transducer (TAM-A, Harvard Apparatus) controlled by a custom Labview program (National Instruments). After the corneoscleral shell was clamped to the pressure chamber, the corneal storage medium was infused into the interior of the shell and applied so it covered the exterior shell surface. The system was purged of all air to prevent bubble formation on the interior cornea surface. One eye from each pair was randomly assigned to the control group (n = 8) or the CXL group (n = 8).

Inflation Testing with Ultrasound Speckle Tracking

A high-frequency (55 MHz) US transducer (Vevo660, Visualsonics, Inc.) was used to acquire acoustic radiofrequency data from the cornea at inflation pressure levels from 5 mm Hg to 45 mm Hg. The raw radiofrequency signal from the cornea was sampled using a digitizer (500 MHz, DP105, Acqiris) and was later used to reconstruct ultrasonic images of the cornea. Before inflation tests, each eye was preconditioned using 5 cycles of pressurization from 5 mm Hg to 45 mm Hg in 60 seconds (Figure 1).

The eye was allowed to equilibrate for 300 seconds at 5 mm Hg and then the pressure was increased to 45 mm Hg using incremental pressurization steps. Specifically, the pressure was increased by 0.5 mm Hg increments from 5 mm Hg to 15 mm Hg followed by increases to pressure levels of 18, 20, 23, 25, 30, 35, 40, and 45 mm Hg. Ultrasound radiofrequency data from the cornea was acquired at each pressure level. Each pressure was held for approximately 1 minute to allow the system to come to equilibrium before the radiofrequency data were obtained. Three repeated inflations were performed to collect radiofrequency data in 3 cross-sections of the cornea as follows: nasal–temporal (N–T),

superior–inferior (S–I), and another direction (A–A) approximately 45 degrees diagonally between these 2 axes (Figure 2). The pressure was slowly decreased back to 5 mm Hg after inflation and allowed to recover for 5 minutes before scanning in a different direction. The order of the scanning directions was randomized for each eye. The inflation tests with US speckle tracking were performed before and after treatment in each eye.

A US speckle tracking algorithm was used to process the radiofrequency data to calculate the distributive strains within the scanned tissue cross-sections.[25] Briefly, the US radiofrequency signals were first filtered using a band-pass filter with a bandwidth of 100 MHz centered at 55 MHz to remove noise. A correlation-based speckle tracking algorithm was then applied to the radiofrequency signals acquired at 2 consecutive pressure levels to compute the displacement vector field within the scanning cross-section. A least-square strain estimator was used to calculate the strains in the axial direction (along the US beam) and lateral direction (perpendicular to US beam). These strains were converted to the radial and tangential strains (Figure 3) based on the transform of the global axial–lateral coordinate to the local radial–tangential coordinate. The average tangential and radial strains across the entire thickness of the cornea were obtained. To assess the through-thickness strain variation, the cornea was divided into 3 concentric equal depth layers (ie, anterior, middle, and posterior third of the cornea). The radial strains and tangential strains in each third of the cornea were then compared before and after treatment.

Corneal Treatment

Immediately before treatment, the epithelium in all corneas was gently removed by scraping with a blunt scalpel blade with IOP maintained at 15 mm Hg. After epithelium removal, riboflavin solution (dextran 20%) was applied at 5-minute intervals for 20 minutes. Corneas in the treatment group were then irradiated for 30 minutes with double UVA diodes (370 nm; 3 mW/cm^2 irradiance) for 30 minutes with continuous application of the riboflavin–dextran solution at 5-minute intervals following the standard clinical protocol. Figure 4 shows a representative eye mounted on an experimental chamber during riboflavin–UVA crosslinking. In the control group, the corneas were not exposed to UVA irradiation but had riboflavin–dextran application every 5 minutes for an additional 30 minutes.

After treatment, the corneas were again covered with corneal storage medium and allowed to equilibrate in this environment for 10 minutes. The inflation test with US speckle tracking (as described above) was then repeated on each cornea in the CXL group and the control group.

Statistical Analysis

Statistical analysis was performed using SAS software (version 9.2, SAS Institute, Inc.). The mean values of the whole-thickness corneal strains were compared before and after treatment in the CXL group and the control group using linear mixed models for repeated measures considering scanning direction (S–I, N–T, A–A) and pressure (10 mm Hg, 20 mm Hg, 30 mm Hg) as covariates. The radial strains and the tangential strains were analyzed separately. Linear mixed models were used to determine whether strains at 20 mm Hg IOP were different in the anterior, middle, and posterior third of the cornea before or after

treatment. The strains in all 16 pretreated eyes (combining the 2 groups) were analyzed using linear mixed models with repeated measures to examine whether there were baseline differences in corneal strains in the 3 scanning cross-sections. A linear mixed model with repeated measures was also used to estimate the corneal thickness changes before and after treatment in the control group and CXL group as well as to detect whether there was a difference in thickness changes between the 2 groups.

RESULTS

Figure 5 shows a typical high-resolution US image reconstructed from the radiofrequency data obtained via the high-frequency US transducer at a frequency of 55 MHz. Figure 6 shows representative corneal strain maps at an IOP of 15 mm Hg before and after CXL.

Figure 7 shows the mean and standard deviation of the whole-thickness tangential and radial strains in all pretreated eyes (n = 16) for each scanning cross-section (S–I, N–T, A–A). No statistically significant difference in radial strains (P=.41) or tangential strains (P=.84) was found between the N–T, S–I, or A–A orientations at an IOP of 20 mm Hg. The strains at other pressure levels also showed no significant difference between the 3 scanning cross-sections.

Comparison of the tangential and radial strains in each third of the cornea (anterior, middle, posterior) in all pretreated eyes showed no statistically significant difference in radial strains between the 3 layers at an IOP of 20 mm Hg (P=.43) (Figure 8). For example, the mean anterior, middle, and posterior radial strains at 20 mm Hg in the N–T cross-section were −0.036 ± 0.019 (SD), −0.033 ± 0.020, and −0.036 ± 0.017, respectively. The tangential strains showed an increasing trend from the anterior cornea to the posterior cornea (anterior < middle < posterior) that was statistically significant (P < .001). For examples, the mean anterior, middle, and posterior tangential strains at 20 mm Hg in the N–T cross-section were 0.017 ± 0.011, 0.021 ± 0.013, and 0.025 ± 0.012, respectively. The results from the S–I and A–A scans were similar (data not shown).

A statistically significant reduction in tangential strains and radial strains was found in the CXL group after treatment (P=.003 and P=.0025, respectively). No significant change in corneal strains was found in the control group (P=.63, radial strains; P=.08, tangential strains). Figure 9 shows an example of strains before treatment and after treatment using data at 20 mm Hg (averaged over all scanning directions). The overall whole-thickness corneal strains were reduced by a mean of 0.012 ±0.007 in tangential strains and 0.016 ± 0.011 in radial strains, representing a 55.0% and 42.0% reduction, respectively, at an IOP of 20 mm Hg (in the N–T scanning cross-section). A small, but statistically insignificant strain reduction occurred in the control group, which was treated with riboflavin only, with a mean overall whole-thickness strain reduction of 0.001 ± 0.005 in tangential strains and 0.001 ± 0.008 in radial strains, a 5.1% reduction and 4.3% reduction, respectively, at an IOP of 20 mm Hg (also in the N–T scanning cross-section). In the CXL group, the mean absolute strain reduction was larger in the anterior third of the cornea than in the posterior third of the cornea (Figure 9, *left*); however, the difference did not achieve statistical significance.

The tangential strains showed a statistically significant layer effect after treatment in the CXL group; that is, the anterior third had the smallest strain, followed by the middle layer and then the posterior layer (P=.023 at 20 mm Hg). No statistically significant difference was found in the radial strains between the corneal layers after treatment in the CXL group (P=.21 at 20 mm Hg). Analyses of the layer effects of strains at other pressure levels yielded similar results. The strain maps in Figure 6 show an example of the reduced tangential and radial strains in the post-CXL corneas, in particular of the tangential strains in the anterior third of the cornea. Figure 10 shows the mean tangential strains and radial strains in each corneal third before and after treatment in the CXL group and the control group. All strain data are from the N–T cross-section.

Table 1 shows the mean pretreatment and posttreatment corneal thickness in both groups, calculated by measuring the average distance between the anterior and posterior boundaries in the US images. The CXL group and the control group had a statistically significant increase in thickness after treatment (P=.013 and P=.006, respectively). The thickness increase was not different between the 2 groups (P=.63).

DISCUSSION

This study showed the potential of using high-frequency US speckle tracking to quantify the heterogeneous mechanical deformations through the thickness of the cornea under physiologic IOP loadings. Our previous work[25] established the accuracy and resolution of this technique in measuring the strains in a scanning cross-section of the ocular shell. This approach is noninvasive and does not require acoustic powers higher than what is used in routine clinical ophthalmic US systems, providing a potential clinical tool to delineate the spatially resolved mechanical responses of the cornea.

The primary finding in this study is the significant reduction of corneal strains in the tangential direction and radial direction in canine eyes after a CXL treatment that resembled the clinical procedure. In addition, we found a significant anterior–posterior gradient in tangential strains in the pretreated fresh canine corneas and the CXL-treated corneas, with a trend toward larger strains at the more posterior site. There was no significant difference in the radial strains from anterior to posterior. We also found that the IOP-induced corneal strains were not different along the N–T, S–I, and in between (A–A) cross-sections. The overall nonlinear relationship between corneal strain and IOP is also of interest, with the cornea appearing to be fairly extensible within normal IOPs (up to approximately 18 mm Hg) and then becoming relatively inextensible above normal physiologic IOPs; this result is consistent with that in a previous study in which corneal strains were estimated from confocal images.[26]

The tangential strains in fresh corneas in this study were similar to those derived from alternative strain measurement methods. For example, tracking reflective markers on rabbit corneal surfaces has yielded tangential strains in the range of 6.0% to 11.0% when the eyes were inflated from 0 mm Hg to 60 mm Hg.[27] Shin et al.[28] found mean tangential strains at the apex of the anterior surface of the human cornea of 1.14% at approximately 35 mm Hg. Hennighausen et al.[26] report mean strains of 1.8% ± 0.1% in the anterior side and 2.1% ±

0.1% in the posterior side of the normally hydrated rabbit cornea at a pressure of 65 mm Hg, showing an anterior to posterior strain gradient similar to that in our study. The general trend toward increased tangential strains on the posterior side of the cornea in these previous reports is also consistent with the larger posterior strains found in the present study.

More specifically, we found that in the pretreated fresh canine corneas, the tangential strains were significantly different in the anterior, middle, and posterior thirds of the cornea. This anterior–posterior gradient in tangential strains is likely an outcome of the differential ECM microstructure from the anterior to the posterior cornea. It is known that the anterior cornea has a higher number of interweaving collagen fibers, providing greater density and higher mechanical stiffness.[29,30] This microstructural organization likely underlies the higher tensile and shear stiffness of the anterior cornea.[31,32] The smaller tangential strains in the anterior third of the canine cornea in our study were consistent with these findings because the stiffer portion of the cornea would be expected to produce smaller strains for a given IOP increase. The anterior–posterior gradient in tangential strains also supports the notion that a significant amount of shear likely occurs during IOP elevations as the cornea lamellae glide past one another.

We found a significant reduction in tangential strains (P=.003) and radial strains (P=.0025) after CXL treatment. The overall corneal strains were reduced by 55% in tangential strains and 42% in radial strains at an IOP of 20 mm Hg (in the N-T cross-section). Using inflation testing on porcine corneas and a model based on changes in the radius of curvature of the cornea, Kling et al.[33] found a similar reduction in tangential strains (ie, approximately 3.0% before CXL and 1.6% after CXL, a 47% reduction). The overall reduction in corneal strains represents a stiffer response of the cornea to IOP inflation (ie, less deformation at physiologic mechanical loadings), confirming the effect of CXL as a means to increase the effective stiffness of the cornea.

After CXL treatment, the tangential strains were also significantly different from the anterior to the posterior third of the cornea. The smallest tangential strain was in the anterior third, followed by the middle third and then the posterior third, showing that the anterior–posterior gradient in the mechanical responses in the pre-treated corneas remained unchanged after crosslinking. This gradient could have been enhanced by the reported attenuation of riboflavin diffusion and UVA penetration over the corneal thickness during CXL treatment; however, the difference in strain reduction between different corneal thirds did not achieve statistical significance in the present study. We did observe that on average, the anterior third of the cornea in the CXL group had the largest reduction in tangential strains; however, the variance across tissue samples was large. It is possible that more superficial CXL (eg, accelerated CXL[34]) may reinforce or accentuate the in-depth gradient of the corneal biomechanical response. The radial strains did not show a significant anterior–posterior gradient in the pretreated corneas or after CXL, and consistently large reductions in radial strains were found in all layers after CXL. This contrast may suggest that the microstructural factors responsible for the radial deformation (ie, compression of the lamellae against each other) are likely different from those for the tangential deformation (ie, stretch along the direction parallel to the corneal curvature).

Although the crosslinking between collagen molecules may explain the reduction in tangential strains, the exact mechanisms behind the radial strain reduction seen in this study are less obvious. It is known that the cornea has a large amount of osmotically active proteoglycan units within its structure. Proteoglycans are thought to be involved in regulating the spacing and organization of the collagen fibrils and thus play an important role in the cornea's optical transparency. Mechanically, proteoglycans are known to be important for resisting compression in tissues, such as articular cartilage.[35] The radial strains in the cornea are compressive in nature (ie, compression through corneal thickness) and thus could be affected by the states of the proteoglycans and their influence on fluid flow in the cornea during compression. Zhang et al.[11] showed in a model reaction system as well as in intact ex vivo corneas that irradiation with UVA in the presence of riboflavin caused not only crosslinking of collagen molecules among themselves and proteoglycan core proteins among themselves but also linkages between collagen and proteoglycan core proteins. Using x-ray scattering, Hayes et al.[36] further showed that the crosslinks formed during CXL occur predominantly at the collagen fibril surface and not within the collagen fibrils. A recent study found an increase of more than 100% in interlamellar cohesive strength after CXL in porcine corneas, suggesting increased interlamellar crosslinking likely due to the linkage between proteoglycans.[37] The crosslinks of proteoglycans among themselves and with collagen molecules may play a role in the decreased radial strains (which were largely compressive) seen in this study in corneas after CXL treatment.

A previous study[38] found the mean healthy in vivo canine cornea thickness to be 598.5 ± 32.38 μm using US pachymetry. Using B-mode US images, our study found a mean canine corneal thickness of 603 ± 44 μm before any treatment, supporting the absence of significant swelling before the start of experimentation. However, a mean increase in corneal thickness of 46.8 ± 29.4 μm and 52.8 ± 31.9 μm was found after treatment in the CXL group and control group, respectively. This mild swelling in the experimental corneas was in contrast to corneal thinning during clinical CXL procedures, although the experimental riboflavin solutions did contain 20.0% dextran. We believe this unexpected swelling likely occurred during the multiple inflations up to a pressure of 45 mm Hg in the ex vivo eyes, in which the corneal endothelium could have been somewhat compromised. The immersion of the corneas in Optisol corneal storage medium (containing only 1.5% dextran) during strain measurements, in particular after epithelium removal, may have also contributed to the swelling seen in this study.

The mild swelling represents a limitation of this study, although its effects did not likely alter the outcome. A previous experiment on ex vivo rabbit corneas[26] found a small reduction in tangential strains in the anterior cornea and a relatively large increase in tangential strains in the posterior cornea when the cornea was swollen. If swelling had the same effect in the canine corneas, the reduction in corneal tangential strains in the anterior cornea after CXL treatment in the present study may partially be due to the mild swelling. The reduction in the posterior tangential strains after CXL, however, was unlikely due to the effects of swelling because the posterior tangential strains would be expected to increase with swelling. It is unclear to what degree swelling may have influenced the radial strains in this study. However, it is important to note that the control group, in which the changes in

corneal thickness were similar to those in the CXL group, had minimal tangential and radial strain reductions throughout the corneal thickness.

The present study used canine eyes as a model system. Both human corneas and canine corneas are slightly ellipsoidal (larger in the horizontal direction). The canine cornea is larger overall relative to the human cornea. The horizontal diameter in the canine cornea ranges from 13 to 17 mm depending on the breed,[39] while the average human cornea horizontal diameter is 11.7 mm.[40] The canine corneas used in this study had a slightly thicker cornea than the average human cornea (603 ± 44 μm versus 536 ± 31 μm[41]). The radius of curvature in the canine cornea has been reported to be approximately 8.5 mm,[42] which is slightly larger than that of human corneas (ie, 7.8 mm).[43] The canine cornea also lacks a Bowman's layer,[44] which has been shown to contribute little to the tensile properties of the human cornea when measured on dissected strips.[45] Furthermore, the human corneal tensile modulus in strip extensiometry testing has been shown to be higher than that of canine corneas, with an average 1% strain secant modulus in human corneas of 2.44 MPa compared with 1.54 MPa in canine corneas.[46] This may result in a larger tangential strain in the canine cornea than in the human cornea for a similar IOP increase.

Other limitations of this study include the following: First, the experiments were performed on the dissected corneoscleral shell, which may be mechanically different from the whole globe. Although the corneoscleral shell was clamped on the posterior third of the sclera to minimize the influence of the clamping on corneal biomechanical responses, future experiments should implement the whole globe setup to avoid deviation from the in vivo boundary conditions. Second, we observed a wide range of strain reductions in the CXL-treated eyes, which was likely due to the different efficacy of the CXL procedure in different eyes even though the same protocol was followed. Future studies should quantify the extent of CXL in each individual eye and identify the corneal strain parameters that best correlate with the extent of CXL. Third, only 3 cross-sectional planes were measured for strain calculations. The very small incremental pressure levels, in particular within the lower pressure range, ensured that the US speckle patterns were highly correlated in the consecutively acquired US data and thus limited the errors due to out-of-plane motion in the strain calculations. In addition, our laboratory is developing 3-D speckle tracking protocols based on high-frequency US to achieve more complete analysis of the regional variations in strains in the entire volume of the cornea.

In conclusion, we found that CXL significantly reduced the tangential strains and radial strains in the cornea. With further modification and optimization, the US strain tracking technique can become a clinical tool for evaluating the spatially resolved corneal biomechanical responses in vivo. Clinical implementation of US speckle tracking techniques has been successful in several areas, including breast cancer detection[47] and liver imaging.[48] Our current high-frequency US system (55 MHz) could achieve a field of view of approximately 8.0 mm in width and 1.0 to 2.0 mm in depth. A possible strategy to acquire strains in vivo is to use those intrinsically present due to the ocular pulse (ie, the cyclic variations in IOP). Other strategies include controlled pressure increases; for example, through the use of a suction cup on the sclera. A coupling fluid or gel will be necessary to transmit the acoustic signals between the transducer and the cornea. In patients, unwanted

ocular movements could present a challenge to accurate strain calculations. Future studies will aim for the clinical translation of this methodology along with its 3-D implementation to characterize in vivo corneal biomechanics.

Acknowledgments

Supported by the National Institutes of Health, Bethesda, Maryland (grant NIHRO1EY020929) and an Ohio State University College of Medicine Research Scholarship. Partially supported by a National Institutes of Health's National Center for Advancing Translational Sciences grant (8UL1TR000090-05) (Dr. Pan).

References

1. Caporossi A, Mazzotta C, Baiocchi S, Caporossi T. Long-term results of riboflavin ultraviolet A corneal collagen cross-linking for keratoconus in Italy: the Siena Eye Cross Study. Am J Ophthalmol. 2010; 149:585–593. [PubMed: 20138607]
2. Wollensak G. Crosslinking treatment of progressive keratoconus: new hope. Curr Opin Ophthalmol. 2006; 17:356–360. [PubMed: 16900027]
3. Sawaguchi S, Yue BY, Sugar J, Gilboy JE. Lysosomal enzyme abnormalities in keratoconus. Arch Ophthalmol. 1989; 107:1507–1510. [PubMed: 2803101]
4. Zhang Y, Mao X, Schwend T, Littlechild S, Conrad GW. Resistance of corneal RFUVA–cross-linked collagens and small leucine-rich proteoglycans to degradation by matrix metalloproteinases. Invest Ophthalmol Vis Sci. 2013; 54:1014–1025. Available at: http://www.iovs.org/content/54/2/1014.full.pdf. [PubMed: 23322569]
5. Greenstein SA, Fry KL, Hersh PS. In vivo biomechanical changes after corneal collagen cross-linking for keratoconus and corneal ectasia: 1-year analysis of a randomized, controlled, clinical trial. Cornea. 2012; 31:21–25. [PubMed: 21993470]
6. Gao XW, Zhao XD, Li WJ, Zhou X, Liu Y. Experimental study on the treatment of rabbit corneal melting after alkali burn with collagen cross-linking. Int J Ophthalmol. 2012; 5:147–150. Available at: http://www.ncbi.nlm.nih.gov/pmc/articles/PMC3359027/pdf/ijo-05-02-147.pdf. [PubMed: 22762039]
7. Makdoumi K, Mortensen J, Crafoord S. Infectious keratitis treated with corneal crosslinking. Cornea. 2010; 29:1353–1358. [PubMed: 21102196]
8. Poli M, Cornut PL, Balmitgere T, Aptel F, Janin H, Burillon C. Prospective study of corneal collagen cross-linking efficacy and tolerance in the treatment of keratoconus and corneal ectasia: 3-year results. Cornea. 2013; 32:583–590. [PubMed: 23086357]
9. Kamaev P, Friedman MD, Sherr E, Muller D. Photochemical kinetics of corneal cross-linking with riboflavin. Invest Ophthalmol Vis Sci. 2012; 53:2360–2367. Available at: http://www.iovs.org/content/53/4/2360.full.pdf. [PubMed: 22427580]
10. McCall AS, Kraft S, Edelhauser HF, Kidder GW, Lundquist RR, Bradshaw HE, Dedeic Z, Dionne MJC, Clement EM, Conrad GW. Mechanisms of corneal tissue cross-linking in response to treatment with topical riboflavin and long-wavelength ultraviolet radiation (UVA). Invest Ophthalmol Vis Sci. 2010; 51:129–138. Available at: http://www.iovs.org/content/51/1/129.full.pdf. [PubMed: 19643975]
11. Zhang Y, Conrad AH, Conrad GW. Effects of ultraviolet-A and riboflavin on the interaction of collagen and proteoglycans during corneal cross-linking. J Biol Chem. 2011; 286:13011–13022. Available at: http://www.jbc.org/content/286/15/13011.full.pdf?with-ds=yes. [PubMed: 21335557]
12. Wollensak G, Spoerl E, Seiler T. Stress-strain measurements of human and porcine corneas after riboflavin–ultraviolet-A-induced cross-linking. J Cataract Refract Surg. 2003; 29:1780–1785. [PubMed: 14522301]
13. Spoerl E, Wollensak G, Seiler T. Increased resistance of cross-linked cornea against enzymatic digestion. Curr Eye Res. 2004; 29:35–40. [PubMed: 15370365]

14. He X, Spoerl E, Tang J, Liu J. Measurement of corneal changes after collagen crosslinking using a noninvasive ultrasound system. J Cataract Refract Surg. 2010; 36:1207–1212. [PubMed: 20610102]
15. Wollensak G, Iomdina E. Long-term biomechanical properties of rabbit corneaafter photodynamic collagen crosslinking. ActaOphthalmol. 2009; 87:48–51. Available at: http://onlinelibrary.wiley.com/doi/10.1111/j.1755-3768.2008.01190.x/pdf.
16. Caporossi, A.; Mazzotta, C.; Baiocchi, S.; Caporossi, T.; Denaro, R. [Accessed November 12, 2013] Age-related long-term functional results after riboflavin UV A corneal cross-linking; J Ophthalmol. 2011. p. article ID: 608041Available at: http://downloads.hindawi.com/journals/jop/2011/608041.pdf
17. Roy AS, Dupps WJ Jr. Patient-specific computational modeling of keratoconus progression and differential responses to collagen cross-linking. Invest Ophthalmol Vis Sci. 2011; 52:9174–9187. Available at: http://www.iovs.org/content/52/12/9174.full.pdf. [PubMed: 22039252]
18. Vinciguerra P, Albè E, Mahmoud AM, Trazza S, Hafezi F, Roberts CJ. Intra- and postoperative variation in ocular response analyzer parameters in keratoconic eyes after corneal cross-linking. J Refract Surg. 2010; 26:669–676. [PubMed: 20438025]
19. Goldich Y, Marcovich AL, Barkana Y, Mandel Y, Hirsh A, Morad Y, Avni I, Zadok D. Clinical and corneal biomechanical changes after collagen cross-linking with riboflavin and UV irradiation in patients with progressive keratoconus: results after 2 years of follow-up. Cornea. 2012; 31:609–614. [PubMed: 22378112]
20. Ford MR, Dupps WJ Jr, Rollins AM, Roy AS, Hu Z. Method for optical coherence elastography of the cornea. J Biomed Opt. 2011; 16:016005. Available at: http://www.ncbi.nlm.nih.gov/pmc/articles/PMC3041813/pdf/JBOPFO-000016-016005_1.pdf. [PubMed: 21280911]
21. Scarcelli G, Pineda R, Yun SH. Brillouin optical microscopy for corneal biomechanics. Invest Ophthalmol Vis Sci. 2012; 53:185–190. Available at: http://www.iovs.org/content/53/1/185.full.pdf. [PubMed: 22159012]
22. Scarcelli G, Kling S, Quijano E, Pineda R, Marcos S, Yun SH. Brillouin microscopy of collagen crosslinking: noncontact depth-dependent analysis of corneal elastic modulus. Invest Ophthalmol Vis Sci. 2013; 54:1418–1425. Available at: http://www.iovs.org/content/54/2/1418.full.pdf. [PubMed: 23361513]
23. Nguyen T-M, Aubry J-F, Touboul D, Fink M, Gennisson JL, Bercoff J, Tanter M. Monitoring of cornea elastic properties changes during UV-A/riboflavin-induced corneal collagen cross-linking using supersonic shear wave imaging: a pilot study. Invest Ophthalmol Vis Sci. 2012; 53:5948–5954. Available at: http://www.iovs.org/content/53/9/5948.full.pdf. [PubMed: 22871840]
24. Hollman KW, Shtein RM, Tripathy S, Kim K. Using an ultrasound elasticity microscope to map three-dimensional strain in a porcine cornea. Ultrasound Med Biol. 2013; 39:1451–1459. [PubMed: 23683407]
25. Tang J, Liu J. Ultrasonic measurement of scleral cross-sectional strains during elevations of intraocular pressure: method validation and initial results in posterior porcine sclera. J Biomech Eng. 2012; 134:091007. erratum 2013, 135, 087001. [PubMed: 22938374]
26. Hennighausen H, Feldman ST, Bille JF, McCulloch AD. Anterior-posterior strain variation in normally hydrated and swollen rabbit cornea. Invest Ophthalmol Vis Sci. 1998; 39:253–262. Available at: http://www.iovs.org/content/39/2/253.full.pdf. [PubMed: 9477981]
27. Jue B, Maurice DM. The mechanical properties of the rabbit and human cornea. J Biomech. 1986; 19:847–853. [PubMed: 3782167]
28. Shin TJ, Vito RP, Johnson LW, McCarey BE. The distribution of strain in the human cornea. J Biomech. 1997; 30:497–503. [PubMed: 9109561]
29. Muller LJ, Pels E, Vrensen GFJM. The specific architecture of the anterior stroma accounts for maintenance of corneal curvature. Br J Ophthalmol. 2001; 85:437–443. Available at: http://www.ncbi.nlm.nih.gov/pmc/articles/PMC1723934/pdf/v085p00437.pdf. [PubMed: 11264134]
30. Winkler M, Chai D, Kriling S, Nien CJ, Brown DJ, Jester B, Juhasz T, Jester JV. Nonlinear optical macroscopic assessment of 3-D corneal collagen organization and axial biomechanics. Invest Ophthalmol Vis Sci. 2011; 52:8818–8827. Available at: http://www.iovs.org/content/52/12/8818.full.pdf. [PubMed: 22003117]

31. Petsche SJ, Chernyak D, Martiz J, Levenston ME, Pinsky PM. Depth-dependent transverse shear properties of the human corneal stroma. Invest Ophthalmol Vis Sci. 2012; 53:873–880. Available at: http://www.iovs.org/content/53/2/873.full.pdf. [PubMed: 22205608]
32. Kohlhaas M, Spoerl E, Schilde T, Unger G, Wittig C, Pillunat LE. Biomechanical evidence of the distribution of cross-links in corneas treated with riboflavin and ultraviolet A light. J Cataract Refract Surg. 2006; 32:279–283. [PubMed: 16565005]
33. Kling S, Remon L, Pérez-Escudero A, Merayo-Lloves J, Marcos S. Corneal biomechanical changes after collagen cross-linking from porcine eye inflation experiments. Invest Ophthalmol Vis Sci. 2010; 51:3961–3968. Available at: http://www.iovs.org/content/51/8/3961.full.pdf. [PubMed: 20335615]
34. Touboul D, Efron N, Smadja D, Praud D, Malet F, Colin J. Corneal confocal microscopy following conventional, transepithelial, and accelerated corneal collagen cross-linking procedures for keratoconus. J Refract Surg. 2012; 28:769–776. [PubMed: 23347370]
35. Buschmann MD, Grodzinsky AJ. A molecular model of proteoglycan-associated electrostatic forces in cartilage mechanics. J Biomech Eng. 1995; 117:179–192. [PubMed: 7666655]
36. Hayes S, Kamma-Lorger CS, Boote C, Young RD, Quantock AJ, Rost A, Khatib Y, Harris J, Yagi N, Terrill N, Meek KM. The effect of riboflavin/UVA collagen cross-linking therapy on the structure and hydrodynamic behaviour of the ungulate and rabbit corneal stroma. PLoS One. 2013; 8:e52860. Available at: http://www.ncbi.nlm.nih.gov/pmc/articles/PMC3547924/pdf/pone.0052860.pdf. [PubMed: 23349690]
37. Tao C, Sun Y, Zhou C, Han Z, Ren Q. Effects of collagen cross-linking on the interlamellar cohesive strength of porcine cornea. Cornea. 2013; 32:169–173. [PubMed: 23172117]
38. Alario AF, Pirie CG. Central corneal thickness measurements in normal dogs: a comparison between ultrasound pachymetry and optical coherence tomography. Vet Ophthalmol. 2013 Epub ahead of print.
39. Gelatt, KN.; Gelatt, JP. Small Animal Ophthalmic Surgery: Practical Techniques for the Veterinarian. Boston, MA: Butter-worth-Heinemann; 2001.
40. Rufer F, Schroder A, Erb C. White-to-white corneal diameter; normal values in healthy humans obtained with the Orbscan II topography system. Cornea. 2005; 24:259–261. [PubMed: 15778595]
41. Doughty MJ, Zaman ML. Human corneal thickness and its impact on intraocular pressure measures: a review and meta-analysis approach. Surv Ophthalmol. 2000; 44:367–408. [PubMed: 10734239]
42. Murphy CJ, Zadnik K, Mannis MJ. Myopia and refractive error in dogs. Invest Ophthalmol Vis Sci. 1992; 33:2459–2463. Available at: http://www.iovs.org/content/33/8/2459.full.pdf. [PubMed: 1634344]
43. Mandell RB, St Helen R. Position and curvature of the corneal apex. Am J Optom Arch Am Acad Optom. 1969; 46:25–29. [PubMed: 5249720]
44. Slatter, DH. Fundamentals of Veterinary Ophthalmology. 3. Philadelphia, PA: Saunders; 2001.
45. Seiler T, Matallana M, Sendler S, Bende T. Does Bowman's layer determine the biomechanical properties of the cornea? Refract Corneal Surg. 1992; 8:139–142. [PubMed: 1591208]
46. Tang J, Pan X, Weber PA, Liu J. Corneal modulus and IOP measurements in canine eyes using Goldmann applanation tonometry and Tonopen. Invest Ophthalmol Vis Sci. 2011; 52:7866–7871. Available at: http://www.iovs.org/content/52/11/7866.full.pdf. [PubMed: 21896862]
47. Hooley RJ, Scoutt LM, Philpotts LE. Breast ultrasonography: state of the art. Radiology. 2013; 268:642–659. Available at: http://pubs.rsna.org/doi/pdf/10.1148/radiol.13121606. [PubMed: 23970509]
48. Canavan C, Eisenburg J, Meng L, Corey K, Hur C. Ultrasound elastography for fibrosis surveillance is cost effective in patients with chronic hepatitis C virus in the UK. Dig Dis Sci. 2013; 58:2691–2704. [PubMed: 23720196]

WHAT WAS KNOWN

- The efficacy of CXL in preventing keratoconus progression has been studied in multiple clinical trials; however, an in vivo method for quantifying the biomechanical changes of the cornea is lacking.

WHAT THIS PAPER ADDS

- This study established the feasibility of using a high-frequency US technique to map the heterogeneous corneal biomechanical responses during IOP elevations as a way to quantify corneal biomechanical changes before and after CXL.

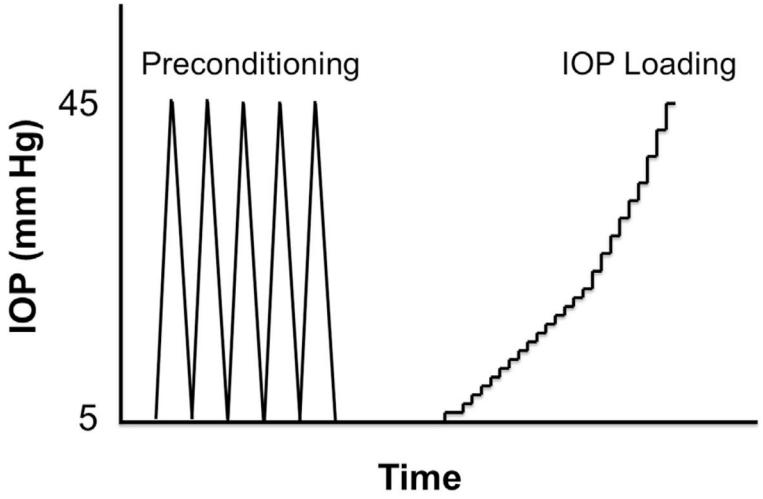

Figure 1.
Inflation testing protocol (IOP = intraocular pressure).

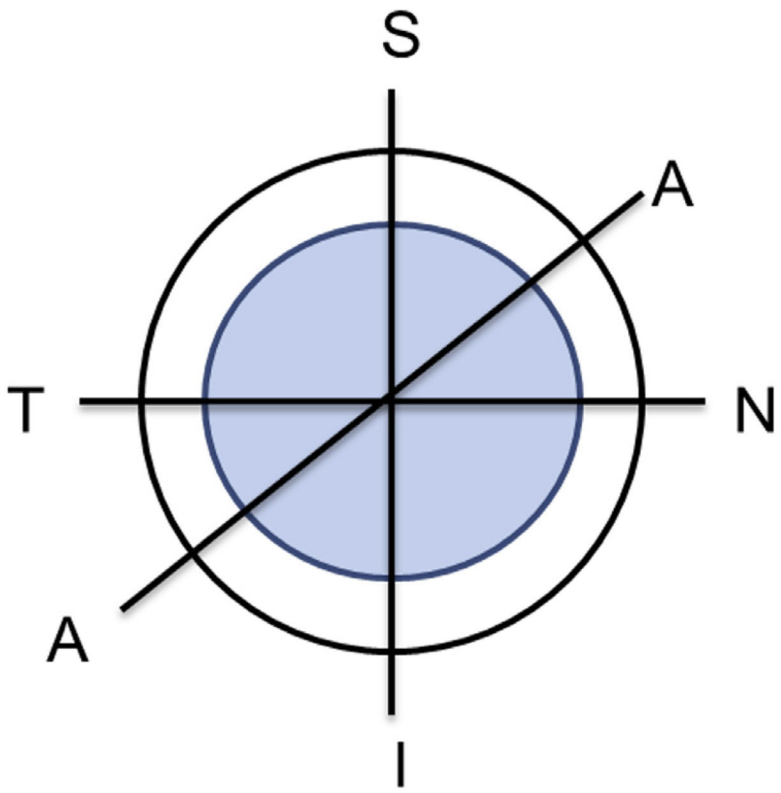

Figure 2.
Location of the 3 cross-sections in which US radiofrequency data were collected (A = direction approximately 45 degrees diagonally between nasal–temporal and superior–inferior; I = inferior; N = nasal; S = superior; T = temporal).

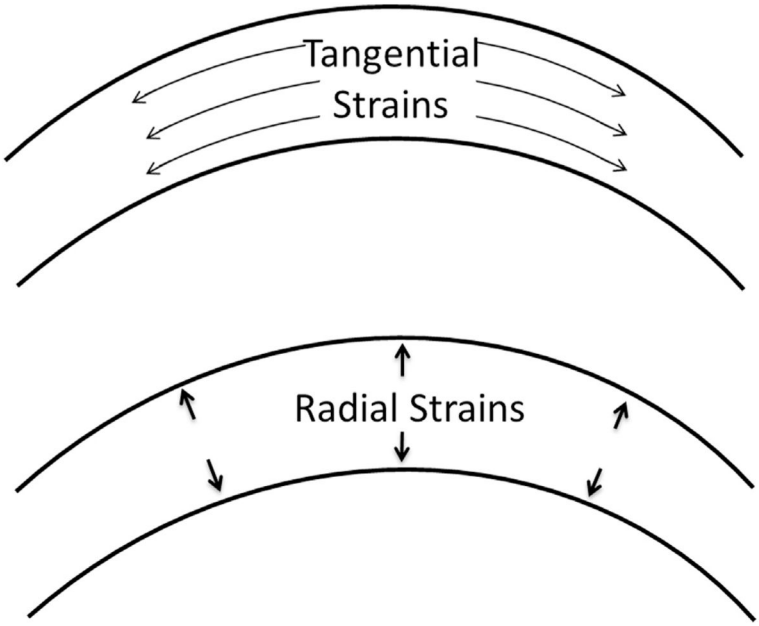

Figure 3.
Corneal tangential strains and radial strains calculated in the study.

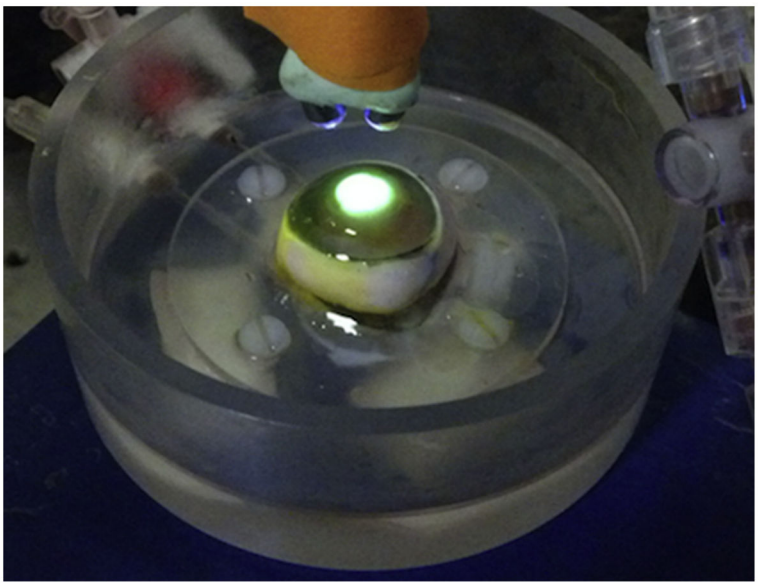

Figure 4.
Canine eye, clamped at the equatorial sclera to the pressure chamber, during CXL.

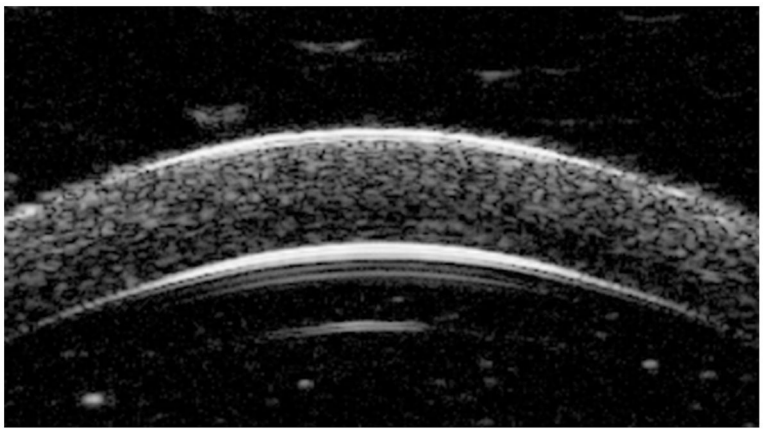

Figure 5.

Ultrasound image reconstructed from the radiofrequency signal of a canine cornea after removal of epithelium shows sufficient speckle patterns throughout the entire cross-section.

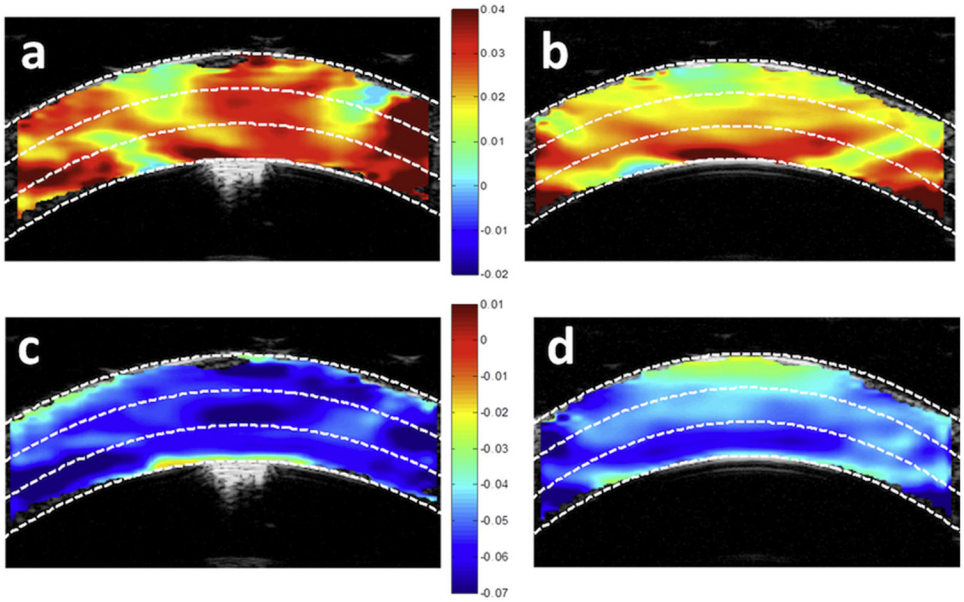

Figure 6.

Strain maps in 1 cornea at an IOP of 15 mm Hg. *a:* Tangential strains before CXL. *b:* Tangential strains after CXL. *c:* Radial strains before CXL. *d:* Radial strains after CXL. The *white dashed lines* illustrate the cutoffs for the anterior, middle, and posterior thirds of the corneal thickness.

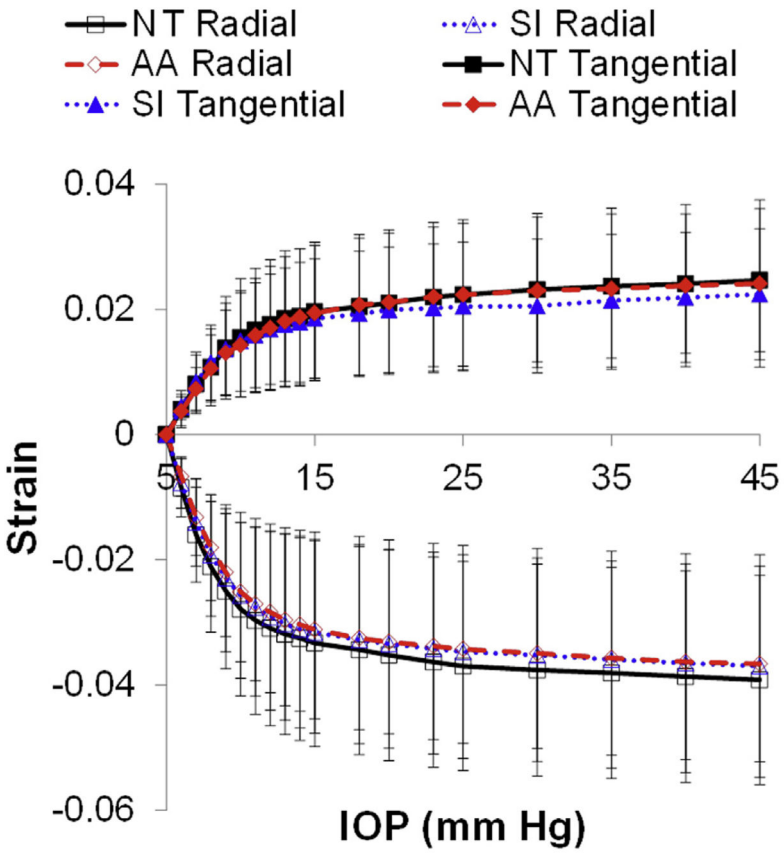

Figure 7.

Mean whole-thickness tangential and radial strains in all pretreated eyes in different scanning cross-sections. The error bar represents standard deviation (AA = direction approximately 45 degrees diagonally between nasal–temporal and superior–inferior; IOP = intraocular pressure; NT = nasal–temporal; SI = superior–inferior).

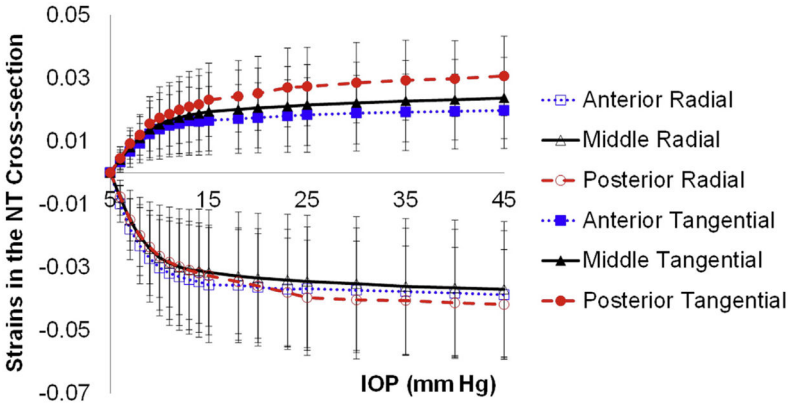

Figure 8.

The tangential and radial strains in each corneal third measured in the N–T cross-section in all pretreated eyes (IOP = intraocular pressure; NT =nasal–temporal).

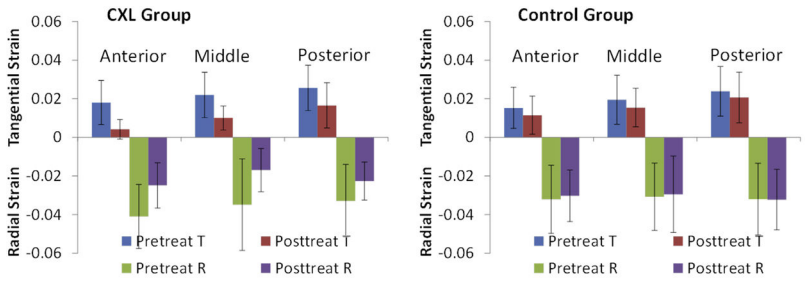

Figure 9.

The mean tangential and radial strains in the anterior, middle, and posterior cornea before and after treatment in the CXL group and control group. Strains at 20 mm Hg and all scanning directions were used (CXL = corneal crosslinking; R = radial; T = tangential).

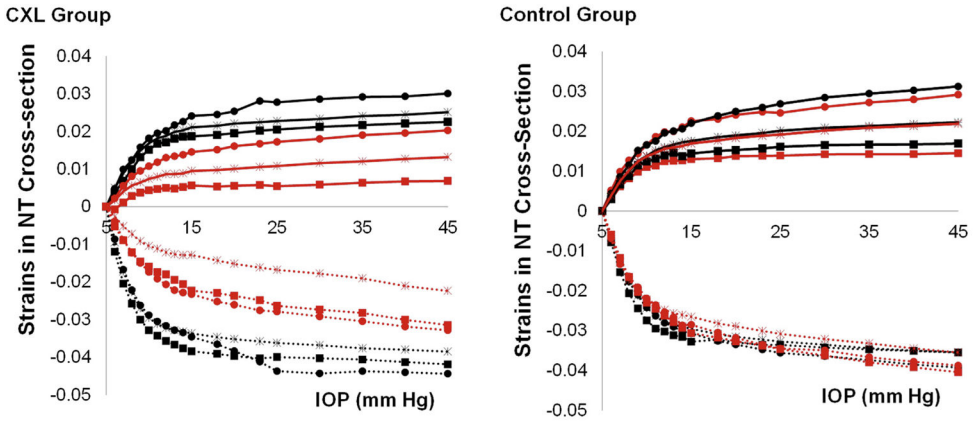

Figure 10.

Tangential and radial strains in the different corneal thirds before and after treatment in the CXL group and control group. The largest reduction in tangential strains was in the anterior cornea in the CXL group. The *black squares* denote the anterior third of the cornea; the *asterisks*, the middle third; and the *black circles*, the posterior third. *Solid lines* represent tangential strains, and *dotted lines* represent radial strains. The *black curves* represent pretreatment strains and the *red curves*, posttreatment strains (CXL = corneal crosslinking; IOP = intraocular pressure; NT = nasal–temporal).

Table 1

Corneal thicknesses before and after treatment in the CXL group and control group measured from 3 scanning cross-sections.

	Mean Corneal Thickness (μm) at IOP of 15 mm Hg ± SD			
	CXL Group		Control Group	
Cross-Section	Before	After	Before	After
N–T	604 ± 44	656 ± 64	599 ± 49	649 ± 42
S–I	608 ± 38	652 ± 66	598 ± 45	648 ± 44
A–A	608 ± 46	652 ± 71	605 ± 47	658 ± 44

A–A = direction approximately 45 degrees diagonally between N–T and S–I; CXL = collagen crosslinking; N–T = nasal–temporal; S–I = superior–inferior